Microstructural Effects on Compressive Behavior and Deformation Band Propagation in Open-Pore Metal Foams

Alexander Martin Matz, Bettina Stefanie Matz and Norbert Jost

Abstract The mechanical properties of investment casted open-pore metal foams are studied on the example of the binary alloy Al–11Zn. The samples are subjected to two different heat treatments, resulting in a state of high strength and low ductility and a state of lower strength and high ductility. Their effects are investigated by compression testing and are correlated to their microstructure. As recently reported in literature, there exist characteristic differences in the stress–strain behavior. This issue has been researched in the course of the present work in detail. We found that it can be directly related to the formation and propagation of deformation bands, and herein locally occurring plastic deformation events. In particular, we observe strength and ductility of the base material in combination with the morphological structure as the dominating factors for the evolution of deformation in metal foams.

Introduction

Metal foams are attractive engineering materials, which combine low weight with a good mechanical strength [1–4]. They have been one of the research highlights in materials engineering ever since the late 80s of the last century [3–9]. The present work is concerned with open-pore metal foams. They consist of a rigid strut network, which defines an interconnected population of cells. The potential of open-pore metal

---

A. M. Matz (✉) · B. S. Matz · N. Jost

Institute for Materials and Material Technologies, Pforzheim University of Applied Sciences, Tiefenbronner Straße 65, Pforzheim 75175, Germany
e-mail: alexander.matz@hs-pforzheim.de

B. S. Matz
e-mail: bettina.matz@hs-pforzheim.de

N. Jost
e-mail: norbert.jost@hs-pforzheim.de

foams in a wide variety of applications has been emphasized in the literature [10–14]. Their mechanical properties are always a determining factor for choosing them as a constructional element. We have recently described how one can make these materials using the model alloy Al–11Zn [15]. We have shown how irreversible plastic strain accumulation occurs during compression testing [16]. We have also demonstrated how the local Al–11Zn microstructure, which evolves during post-processing heat treatments, affects the macroscopic mechanical behavior of an open-pore metal foam during compression testing [17]. The microstructure mainly defines the deformation behavior of bulk material. In foams, it is additionally affected by the structural architecture of the cellular material leading to their capability to effectively dissipate energy under compressive loading. The stress–strain curves of metal foams under compressive loading show the three typical stages of formation:

(1) elastic–plastic region,
(2) plateau region, and
(3) densification region,

as commonly described in literature [2, 18–20]. During compressive loading of the specimen, we preferentially observe a localization of plastic strain in single struts. They underlie such a pronounced deformation that single foam cells collapse and one or a few deformation bands form throughout the entire foam [21]. The stress–strain curve in most cases indicates the initial cell collapse [4] (the corresponding stress is referred to as plastic collapse stress σ_{PC}). It shows a local maximum (which separates the elastic–plastic and the plateau region) due to the sudden stress drop caused by a failing strut. This is characteristic of metal foams subjected to compressive loading, and it is higher the more brittle the base material, such as the aluminum alloy AA6101 in aged conditions [21, 22]. Ductile materials, such as Al in a chemical purity of 99.99% or Al–12Si [23–25], rather show a smooth transition of the elastic–plastic to the plateau regime of the stress–strain curve. Besides the base materials, the thermal treatment seems to be another parameter affecting this behavior [17, 26].

From what has been outlined so far, it is clear that the microstructure and the structural architecture of the cellular material are the factors dominating the fashion of the stress–strain curves. The stress–strain curves are, however, just what we gain from the test procedure; and this is actually a result of the deformation process taking place within the specimen in general. For a profound understanding of the underlying correlations, we manufacture open-pore Al–11Zn foams and apply two different heat treatments. Furthermore, we investigate the evolution of deformation in the foams during compressive loading and observe significant effects of the microstructure on the deformation band propagation during compressive loading.

Experimental Procedure

The material used was the binary aluminum alloy Al–11Zn. It was alloyed by HMW Hauner Metallische Werkstoffe from Al and Zn, each with a nominal purity of 99.99%. The materials are the same as those used by Matz et al.; for details of the chemical composition, refer to [16].

Open-pore Al–11Zn foams were fabricated through a modified investment casting process. Description, that is more detailed, can be found in [15]. Casting was carried out by a centrifugal casting machine of the type Vacutherm-3,3-Titan from Linn High Therm GmbH using a crucible of the type DKV-2 LT. Subsequent to casting, the molds containing the samples were water-quenched. Mold removal and cleaning of the samples were carried out in a water jet machine of the type HW 70 from KWS Kächele GmbH, and afterward by a chemical treatment in tetranatriumethylendiamintetraacetate ($C_{10}H_{12}N_2Na_4O_8$). Samples were cut in dimensions of $30 \times 30 \times 20$ mm^3 by wire electro-discharge machining [27]. A homogenization treatment at a temperature of $T = 400$ °C lasting $t = 120$ min in connection with water-quenching was applied to all samples. Half of them were aged at room temperature (samples *A(RT)*) to achieve finely dispersed GP zones [28]. The rest pass through an additional annealing treatment at a temperature of $T = 150$ °C for $t = 120$ min (samples *A (150/120)*) in order to obtain a microstructure with partially dissolved GP zones. Details on the effects of heat treatments on the microstructure are described elsewhere [17]. The pore density of all samples was $\rho_P = 10$ ppi, and the relative density was in a range of $7.5\% \le \rho_{rel} \le 11.0\%$.

Uniaxial compression tests were performed with a TesT universal test rig P112.20 KN.H at room temperature and ambient air. The displacement rate was set to be 0.9 mm/min, which corresponds to an initial strain rate of 5×10^{-4} s^{-1}. Precision-grinded steel plates (coated by a graphite lubricant) were used to apply compression forces to the samples (Fig. 1). The testing procedure was documented with a camera
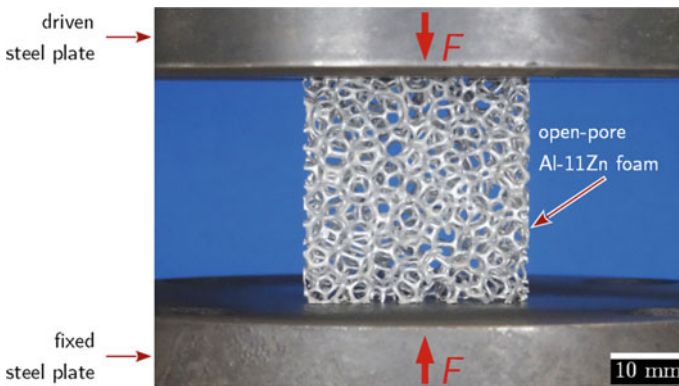

Fig. 1 Experimental setup for compression tests of open-pore Al–11Zn foams, which corresponds to the setup described in Ref. [16]

of the type Cyber-SHOT DSC-HX50V from Sony, Corp. in order to evaluate the evolution of deformation within the whole foam specimen. Furthermore, close-up views of relevant parts of the deformed samples were taken with a digital microscope (VHX 500FD from Keyence NV/SA).

Results

Compressive Properties

The stress–strain curves (Fig. 2) of the foams under compressive loading show in general the three abovementioned typical stages of formation. At the beginning of deformation, the samples aged at room temperature have a linear increase in stress. Thereafter, we notice an increasing portion of plasticity, which is a consequence of strain hardening [16], until the tangent modulus turns zero, when reaching the plastic collapse strain σ_{PC}. The plateau region follows up, when a sudden stress drop occurs and subsequently continues as an oscillating curve. At higher strains, the distinct rise in stress can be identified as densification region. The other samples, which passed through an additional annealing treatment at a temperature of $T = 150\ °C$, exhibit a different curve fashion with the characteristic smooth transition from the elastic–plastic region into the plateau region. The strain at which the transition occurs is hard to judge, but it is in an order of $\varepsilon \approx 10\%$ as also reported previously for ductile Al foams [24]. In contrast to the samples aged at room temperature, no oscillating fashion of the curve can be detected in the plateau region. The densification of the foams is mainly a function of relative density [17, 18] and is, hence, in the same order as the samples *A(RT)*.

Fig. 2 Compressive stress–strain behavior of open-pore Al–11Zn foams in heat treatment conditions *A(RT)* and *A(150/120)*
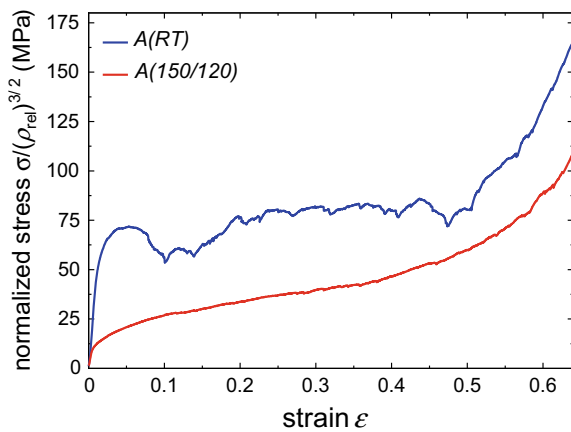
Local Deformation Behavior

Compressive loading of open-pore Al–11Zn foams leads to a preferably local for-mation of deformation bands. Within the concerned specimen areas, single struts are deformed to such a high extent until a fatal collapse of the corresponding cell occurs and/or until the locally reached strain hardening leads to spreading of the deformation band into prior non-effected specimen areas. Figure 3a–c shows how the deformation in an open-pore Al–11Zn foam aged at room temperature evolves on the example of different deformation stages. The corresponding stress–strain diagram is shown in Fig. 3g. The deformation bands, which are active in the different deformation stages, and the hitherto initiated fractures are labeled in the images. The sample displayed in Fig. 3a resamples the reference state at a strain of $\varepsilon = 0$ immediately before the compression test started. When applying compressive loading, at first, a homogenous deformation within the whole specimen occurs, which still seems to be accompanied by a portion of elastic strain ($\varepsilon \leq 1.37\%$). Thereafter, a first deforma-tion band forms and arranges in the upper part of the sample oriented in an angle of $\alpha \approx 20°$ across the direction of force application. A further deformation band forms when reaching a strain of $\varepsilon \leq 3.55\%$ oriented in an angle of $\alpha \approx 15°$ across the direction of force application. It is located in the lower part of the sample and it is connected near the left sample surface with the first deformation band formed (this state is shown in Fig. 3b at a strain of $\varepsilon = 6.50\%$). The deformation itself, however, is still restricted to the deformation band, which is located in the upper part of the specimen. Within this band and in the direct adjoining parts, fractures of the struts occur, which are labeled by arrows in Fig. 3b. At a nominal strain of $\varepsilon = 5.32\%$, the ongoing deformation of the sample is of the same order in both active defor-mation bands. Not before reaching $\varepsilon = 8.22\%$, the main deformation shifts to the deformation band, which is located in the lower part of the specimen. This defor-mation band is distinctively silhouetted against the sample parts above and below. Furthermore, fracture initiation and fracture occur within the deformation bands and at adjacent regions where the strut orientation itself leads to a highly rigid structure, and hence restrains plastic deformation (this state is shown in Fig. 3c at a strain of $\varepsilon = 11.04\%$). Afterward, entire cell planes, containing the afore fractured struts, collapse and the deformation band spreads into regions of the sample at which no prior macroscopic deformation could be observed. In direct comparison to the sam-ple in cold-aged condition, the progressive deformation behavior of the sample in the condition with partially dissolved GP zones is shown in Fig. 3d–f. The corre-sponding stress–strain diagram is displayed in Fig. 3h. Figure 3d shows the initial state at a strain of $\varepsilon = 0$. When compression testing started, in the first instance (as well as observed in the cold-aged condition), the sample deforms homogeneously. Subsequently and as a gradual process, the deformation events get concentrated in the middle of the sample. Correspondingly, at parts of the sample, which are in direct contact with the compression plates, minor deformation occurs, and when reaching a strain of $\varepsilon = 5.79\%$ no deformation events can be observed anymore. Thereupon, an increasing localization in the form of a distinctly wide shaped deformation band
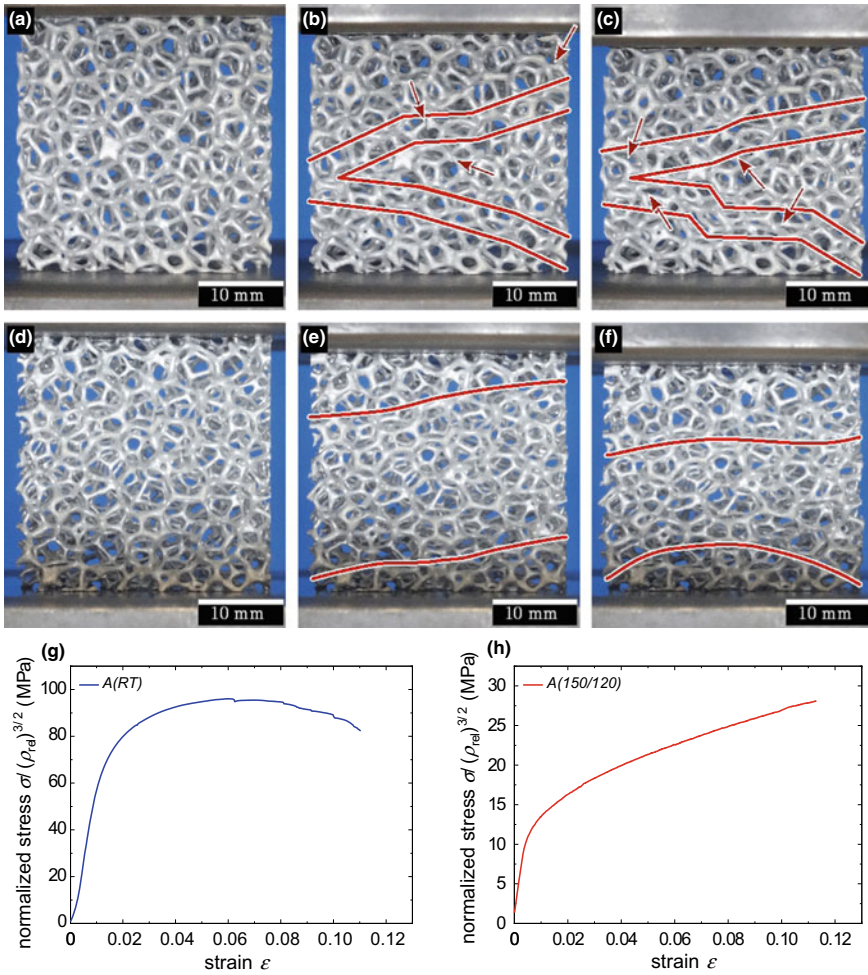
Fig. 3 Formation and propagation of deformation bands, and fracture initiation during compression testing of open-pore Al–11Zn foams: **a** reference state ($\varepsilon = 0$), **b** compressed to $\varepsilon = 6.50\%$, **c** compressed to $\varepsilon = 11.04\%$, and **g** corresponding stress–strain behavior of sample *A(RT)*, as well as **d** reference state ($\varepsilon = 0$), **e** compressed to $\varepsilon = 6.32\%$, **f** compressed to $\varepsilon = 11.29\%$, and **h** corresponding stress–strain behavior of sample *A(150/120)* (deformation bands are marked by lines and fractures are marked by arrows)

can be noticed, which stretches across about ¾ of the sample height (this state is shown in Fig. 3e at a strain of $\varepsilon = 6.32\%$). At $\varepsilon \approx 7.39\%$, the deformation band gradually relocates into the lower third of the sample. The major deformation events proceed in the center of the deformation band. When reaching a strain of $\varepsilon \approx 8.37\%$, the deformation stagnates in the lower part of the sample and the deformation band starts shifting upward. Ongoing strain intensifies this behavior as can be seen in Fig. 3f ($\varepsilon \approx 11.29\%$) and leads to a pronounced bending of single struts until they

finally touch each other. Not before a compaction of the affected cell planes occur, the deformation band relocates into sample parts, which are macroscopically much less deformed.

The deformation events in both samples differ totally as pointed up in Fig. 4. The cold-aged sample is considerably more brittle. It shows a pronounced sensitivity to fracture events as illustrated in Fig. 4b (this is a detail view of Fig. 4a, which corresponds to the final state of compression of the cold-aged sample, as shown in Fig. 3c). The highlighted fracture *I* is the result of a shearing dominated strain, whereas fractures *II* and *III* are the consequence of bending-dominated strain. The sample in the condition with partially dissolved GP zones is considerably ductile in contrast to the cold-aged sample. Prior to the collapse of the first cell plane, no fractures can be detected. We rather observe a pronounced local plastic deformation, as shown in the marked region of the sample in Fig. 4c. A detail view of the relevant strut (which
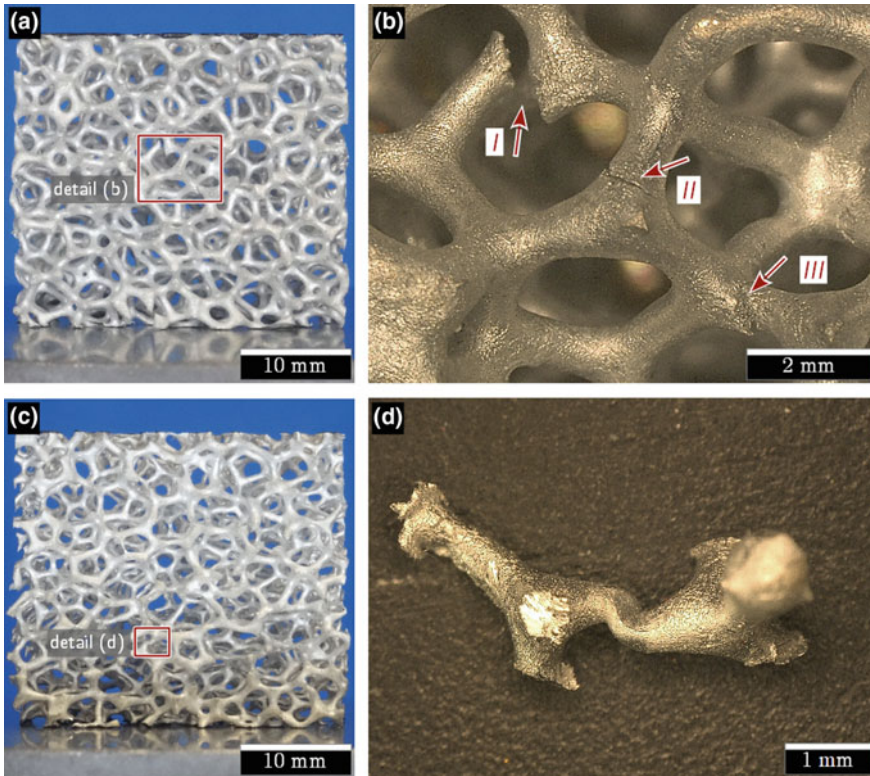

Fig. 4 Deformation phenomena of struts within a deformation band of open-pore Al–11Zn foams: **a** sample *A(RT)* compressed to $\varepsilon = 11.04\%$ (cf. Fig. 3c), **b** close-up view of labeled sample area in (**a**), **c** sample *A(150/120)* compressed to $\varepsilon = 11.29\%$ (cf. Fig. 3f), and **d** close-up view of labeled sample area in (**c**)

was extracted for better presentation) is displayed in Fig. 4d. The alteration of shape
is clearly visible and likewise a result of shearing dominated strain.

Discussion

The deformation of open-pore metal foams relies on the formation of local defor-
mation bands. Regarding both microstructures considered in the present study, we
clearly observe differences in shape and in propagation of the deformation bands
during compressive loading. At the beginning, the deformation band in the specimen
A (150/120) nearly involves the whole sample. It localizes or concentrates gradually
as a function of strain ε (cf. Fig. 3e, f). This behavior also becomes noticeable in the
stress–strain diagram (cf. Fig. 2) at which a continuous increase of stress σ occurs in
the plateau region. It is a consequence of the strain hardening of the base material. It
seems that the sample areas, which are next to the compression plates, firstly under-
lie a strain hardening which spreads into the center of the specimen as a function of
strain ε. Against this background, we notice a strain hardening rate $k_{Pl} = d\sigma / d\varepsilon$
in the plateau region of $k_{Pl} = 1.7$ MPa [17]. In contrast, the strain hardening rate in
the plateau region is only about two-thirds of that in the specimen *A(RT)* [17]. Its
deformation bands (one or more) are formed in a dimension of approximately one
cell plane in the specimen *A(RT)* (cf. Fig. 3b, c). The deformation band concentrates
locally right from the outset, as numerously reported in literature for metal foams
with open and closed cells [20, 21, 29–32]. Strain hardening takes place within the
affected specimen area until single struts fracture. This leads to a local structural
softening of the foam and in consequence to an oscillating behavior of the stress–
strain curve (cf. Fig. 2). Based on this, we conclude that during compression loading,
there is a prior base material controlled strain hardening in the specimen *A (150/120)*,
whereas there is an interrelated strain hardening of base material and softening of
foam structure in the specimen *A(RT)*.

The deformation bands are in general oriented in an angle of $15° \leq \alpha \leq 20°$
transverse to the direction of applied compressive force as also reported previously
[29, 31, 33]. In analogy to slip planes in crystals, we interpret this phenomenon to be
related to the packing of the polydisperse foam's polyhedral cells in space but here
on the mesostructural scale. The deformation itself is concentrated on the weakest
part of the foam and evolves with increasing nominal strain ε by

(1) deformation of single struts to such an extent that a collapse of the belonging
     cell occurs,
(2) a pronounced local strain hardening of the bulk material, and/or
(3) a local hardening of the foam structure itself, which is related to a geometri-
     cal beneficial arrangement of partially deformed struts being more stable than
     adjacent specimen parts.

The aspects (1) and (3) are the major active mechanisms for the formation and propagation of deformation bands in samples *A(RT)*, whereas (2) and (3) are predominant in the samples *A(150/120)*. This explains on the one hand the differing shapes of the deformation bands (Fig. 3) and on the other hand their characteristic stress–strain curve behaviors, such as a noticeable plastic collapse in *A(RT)* samples or a noticeable linear strain hardening rate in the plateau region in *A(150/120)* samples.

Conclusion

In the present study, we investigate how the microstructure of Al–11Zn affects the compressive behavior and deformation band propagation in open-pore metal foams. From the results obtained in this work, the following main conclusions can be drawn:

(1) The major deformation events concentrate on one or a few parts of the sample (deformation bands) until either a collapse of the cell plane occurs resulting in a structural softening of the foam or the foam's base material undergoes a strain hardening to such an extent that the deformation migrates to an adjacent weaker part and further deformation band propagation gets activated;

(2) In a metal foam with brittle base material, the deformation locally remains until fracture of struts and/or collapse of cells or cell planes occur—its deformation is dominated by structural softening;

(3) In a metal foam with ductile base material, the deformation is rather homogenous within the whole sample and gradually localizes in a deformation band as a function of strain—its deformation is dominated by strain hardening of its base material.

References

1. Ashby MF (1983) The mechanical properties of cellular solids. Metall Trans A 14(9):1755–1769
2. Banhart J, Baumeister J (1998) Deformation characteristics of metal foams. J Mater Sci 33(6):1431–1440
3. Banhart J (2013) Light-metal foams—history of innovation and technological challenges. Adv Mater Eng 15(3):82–111

4. Gibson LJ (2000) Mechanical behavior of metallic foams. Annu Rev Mater Sci 30(1):191–227
5. Ashby MF, Evans A, Fleck NA, Gibson LJ, Hutchinson JW, Wadley HNG (2000) Metal foams—a design guide. Butterworth-Heinemann, Woburn
6. Banhart J (2001) Manufacture, characterisation and application of cellular metals and metal foams. Prog Mater Sci 46(6):559–632
7. Gibson LJ, Ashby MF (2001) Cellular solids: structures and properties. Cambridge University Press, Cambridge
8. Lefebvre L-P, Banhart J, Dunand DC (2008) Porous metals and metallic foams: current status and recent developments. Adv Mater Sci 10(9):775–787
9. Dukhan N (ed) (2013) Metal foams: fundamentals and applications. DEStech Publications, Lancaster
10. Han X-H, Wang Q, Park Y-G, T'joen C, Sommers A, Jacobi A (2012) A review of metal foam and metal matrix composites for heat exchangers and heat sinks. Heat Transf Eng 33(12):1–20
11. Zhao CY (2012) Review on thermal transport in high porosity cellular metal foams with open cells. J. Heat Mass Transfer 55(13–14):3618–3632
12. Betts C (2012) Benefits of metal foams and developments in modelling techniques to assess their materials behaviour: a review. Mater Sci Technol 28(2):129–143
13. Müller DW, Matz AM, Jost N (2013) Casting open porous Ti foam suitable for medical applications. Bioinsp Biomim Nanobiomater 2(2):76–83
14. Yang G-F, Song K-Y, Joo S-K (2015) Ultra-thick Li-ion battery electrodes using different cell size of metal foam current collectors. RSC Adv 5:16702–16706
15. Matz AM, Mocker BS, Müller DW, Jost N, Eggeler G (2014) Mesostructural design and manufacturing of open-pore metal foams by investment casting. Adv Mater Sci Eng 2014(421729):1–9
16. Matz AM, Matz BS, Jost N, Eggeler G (2018) On the accumulation of irreversible plastic strain during compression loading of open-pore metallic foams. Mater Sci Eng A 728:40–44
17. Matz AM, Matz BS, Parsa AB, Jost N, Eggeler G (2019) On the effects of microstructure on the mechanical properties of open.pore Al-11Zn foams. Mater Sci Eng A 759:552–564
18. Matz AM (2017) Werkstoff-und morphologieabhängige Einflüsse auf die mechanischen Eigenschaften von offenporigen Al-11Zn-Schäumen. Shaker, Herzogenrath
19. Miller RE (2000) A continuum plasticity model for the constitutive and indentation behaviour of foamed metals. Int J Mech Sci 42(4):729–754
20. Schüler P, Fischer SF, Bühring-Polaczek A, Fleck C (2013) Deformation and failure behaviour of open cell Al foams under quasistatic and impact loading. Mater Sci Eng A 587:250–261
21. Jang WY, Kyriakides S (2009) On the crushing of aluminum open-cell foams: Part I experiments. Int J Solids Struct 46(3):617–634
22. Zhou J, Shrotriya P, Soboyejo WO (2004) Mechanisms and mechanics of compressive deformation in open-cell Al foams. Mech Mater 36(8):781–797
23. Despois J-F, Mueller R, Mortensen A (2006) Uniaxial deformation of microcellular metals. Acta Mater 54(16):4129–4142
24. San Marchi C, Mortensen A (2001) Deformation of open-cell aluminum foam. Acta Mater 49(19):3959–3969
25. San Marchi C, Despois J-F, Mortensen A (2004) Uniaxial deformation of open-cell aluminum foam: the role of internal damage. Acta Mater 52(10):2895–2902
26. Zhou J, Gao Z, Cuitino AM, Soboyejo WO (2004) Effects of heat treatment on the compressive deformation behavior of open cell aluminum foams. Mater Sci Eng A 386(1–2):118–128
27. Matz AM, Kammerer D, Jost N, Oßwald K (2016) Machining of metal foams with varying mesostructure using Wire EDM. Proc CIRP 42:263–267
28. Garwood RD, Davies AL (1960) The effect of structural imperfections on the age-hardening of aluminium-zinc alloys. J Inst Met 88(7):311–317
29. Bart-Smith H, Bastawros AF, Mumm DR, Evans AG, Sypeck DJ, Wadley HNG (1998) Compressive deformation and yielding mechanisms in cellular Al alloys determined using X-ray tomography and surface strain mapping. Acta Mater 46(10):3583–3592

30. Bastawros A-F, Bart-Smith H, Evans AG (2000) Experimental analysis of deformation mechanisms in a closed-cell aluminum alloy foam. J Mech Phys Solids 48(2):301–322
31. Mu Y, Yao G, Liang L, Luo H, Zu G (2010) Deformation mechanisms of closed-cell aluminum foam in compression. Scripta Mater 63(6):629–632
32. Mukherjee M, Kolluri M, Garcia-Moreno F, Banhart J, Ramamurty U (2009) Strain hardening during constrained deformation of metal foams—effect of shear displacement. Scripta Mater 61(7):752–755
33. Kolluri M, Karthikeyan S, Ramamurty U (2007) Effect of lateral constraint on the mechanical properties of a closed-cell al foam: I experiments. Metall Mater Trans A 38(9):2006–2013